# Individual tree detection and estimation of stem attributes with mobile laser scanning along boreal forest roads

Raul de Paula Pires [*], Kenneth Olofsson, Henrik Jan Persson, Eva Lindberg, Johan Holmgren

*Dept. of Forest Resource Management, Swedish University of Agricultural Sciences, Umeå, Sweden*

## ARTICLE INFO

## ABSTRACT

The collection of field-reference data is a key task in remote sensing-based forest inventories. However, traditional methods of collection demand extensive personnel resources. Thus, field-reference data collection would benefit from more automated methods. In this study, we proposed a method for individual tree detection (ITD) and stem attribute estimation based on a car-mounted mobile laser scanner (MLS) operating along forest roads. We assessed its performance in six ranges with increasing mean distance from the roadside. We used a Riegl VUX-1LR sensor operating with high repetition rate, thus providing detailed cross sections of the stems. The algorithm we propose was designed for this sensor configuration, identifying the cross sections (or arcs) in the point cloud and aggregating those into single trees. Furthermore, we estimated diameter at breast height (DBH), stem profiles, and stem volume for each detected tree. The accuracy of ITD, DBH, and stem volume estimates varied with the trees' distance from the road. In general, the proximity to the sensor of branches 0–10 m from the road caused commission errors in ITD and over estimation of stem attributes in this zone. At 50–60 m from roadside, stems were often occluded by branches, causing omissions and underestimation of stem attributes in this area. ITD's precision and sensitivity varied from 82.8% to 100% and 62.7% to 96.7%, respectively. The RMSE of DBH estimates ranged from 1.81 cm (6.38%) to 4.84 cm (16.9%). Stem volume estimates had RMSEs ranging from 0.0800 m$^3$ (10.1%) to 0.190 m$^3$ (25.7%), depending on the distance to the sensor. The average proportion of detected reference volume was highly affected by the performance of ITD in the different zones. This proportion was highest from 0 to 10 m (113%), a zone that concentrated most ITD commission errors, and lowest from 50 to 60 m (66.6%), mostly due to the omission errors in this area. In the other zones, the RMSE ranged from 87.5% to 98.5%. These accuracies are in line with those obtained by other state-of-the-art MLS and terrestrial laser scanner (TLS) methods. The car-mounted MLS system used has the potential to collect data efficiently in large-scale inventories, being able to scan approximately 80 ha of forests per day depending on the survey setup. This data collection method could be used to increase the amount of field-reference data available in remote sensing-based forest inventories, improve models for area-based estimations, and support precision forestry development.

## 1. Introduction

The first studies that used ground-based LiDAR (Light Detection and Ranging) to measure forests date from the early 2000 s (Hopkinson et al., 2004; Lovell et al., 2003). Since then, different authors have explored and reported on the accuracy of stationary (Terrestrial Laser Scanner – TLS) and mobile (Mobile Laser Scanner – MLS) ground-based LiDAR to measure forest parameters and stem attributes. These systems can provide accurate measurements of stem profiles and diameter at breast height (DBH) at tree-level in a relatively short time and with

centimeter-level accuracy (Balenović et al., 2020; Hyyppä et al., 2020c; Olofsson and Holmgren, 2016; Pierzchała et al., 2018; Puliti et al., 2020). In addition, some ground-based laser systems can go beyond estimation of traditional plot-level attributes (Newnham et al., 2015) and provide, for instance, information on trees' branch structure (Lau et al., 2018; Zhang et al., 2020) and sawmill timber quality (Pyörälä et al., 2019b, 2019a) with good accuracy and a high level of detail.

However, ground-based LiDAR systems are not operationally used in forest inventory despite their proven suitability for retrieving field data due to different reasons, for instance, the high prices of the equipment

and the availability of data processing tools. In addition, the intensive manual work required for collection of TLS and MLS data (Calders et al., 2020), with field campaigns comparable to those of traditional forest inventory, make these technologies less competitive with traditional methods.

Area-based approaches (ABA, Næsset 2002) have been used in many operational remote sensing-based forest inventories, providing estimates for a given region or pixel that can vary in size from a few square meters to hectares (Holopainen et al., 2014). In this approach, field-reference data are used as a response variable in the calibration of remote sensing-based models. Such models can be used to estimate forest attributes, such as timber volume per hectare, over the entire inventoried area. To develop a good model, the reference data should be representative of the whole study area, covering as much of the forest variability as possible. However, drawing a sample that sufficiently represents the whole inventoried area is time- and resource-consuming, which causes surveys to be a trade-off between cost efficiency and accuracy gain. The ABA has been used in simple homogenous forest conditions such as Scandinavian forests to provide rather accurate stand-level estimates. However, such estimates usually lack the details necessary for optimal planning of forest usage for different goals, such as tree-level information (Holopainen et al., 2014). Hence, the term Precision Forestry has been introduced and is often used to describe the stage at which individual tree maps are generated (Hyyppä et al., 2020c), including both qualitative (e.g., species) and quantitative (e.g., diameter and volume) information about each tree. This stage requires efficient methods for collecting reference data in an amount sufficient to train models at the individual tree level.

Recently, MLS systems appeared as efficient alternatives to conduct forest measurements (Holmgren et al., 2019; Hyyppä et al., 2020b; Liu et al., 2021; Puliti et al., 2020). They can be grouped according to their platform, namely handheld, on a backpack, or vehicle- or UAV-mounted (also called ULS). One important challenge of using MLS is the positioning signal under the forest canopy, which makes the co-registration of the point clouds a challenge to be solved by different methods (Bakula et al., 2015; Kukko et al., 2017; Qian et al., 2017). Improvements in the accuracy of positioning under forest canopy, and in the LiDAR sensor technology, have made it possible to acquire MLS point clouds comparable with those obtained with TLS in terms of accuracy and precision. For instance, Hyyppä et al. (2020c) obtained point clouds with point registration accuracies ranging from $\pm$ 1 cm in a backpack MLS to $\pm$ 3 cm in a handheld MLS and under canopy ULS.

Amongst the different MLS systems, the ones mounted on all-terrain vehicles (ATVs) or cars are used in the assessment of some types of urban infrastructure and by the automotive industry (Puente et al., 2013), but less often in forestry compared to TLS or other MLS systems. This system has a great potential to be used in automatic large-scale forest assessments and to provide an alternative to traditional reference data collection. Nevertheless, only a few promising studies have assessed its suitability to measure forest structure at individual tree-level. For instance, Forsman et al. (2016) proposed an algorithm to detect stem points in a point cloud acquired from a car-mounted MLS, yielding an RMSE (Root Mean Squared Error) of 3.7 cm on DBH estimations. Later, Čerňava et al. (2019) tested the performance of a highly accurate MLS mounted on a tractor under heavy canopy conditions, reporting an RMSE of 3.1 cm on DBH estimations in these areas. Both studies suggest that vehicle-mounted MLS could be used to conduct forest measurements.

A car-mounted MLS can provide reference data in the quantity and quality required to calibrate models at individual tree level and reduce the need of labor-intensive field campaigns, thus supporting efficient Precision Forestry. This system can take advantage of forest road networks in regions like Sweden, where there are approximately 210,000 km of forest roads accounting for about one-third of the total road network in the country (Axelsson et al., 2018), making measurements on the go during field visits or operations. However, areas with dense forest

cover and sparse road network could not be suitable for using of a vehicle-mounted MLS with inventory purposes, once the sampling would be restricted to only a few areas. In terms of autonomy, cars or ATVs are capable of operating for longer during field campaigns when compared to other MLS systems (e.g., under-canopy ULS). Moreover, it would be possible to train models with local reference data in remote sensing-based forest inventory, instead of using samples at the regional or national level. Finally, the smooth trajectory on forest roads together with a clear positioning signal can yield high accuracy point clouds, making it possible to derive accurate estimates of forest variables at individual tree level.

A method able to estimate stem attributes using MLS from forest roads could change the current opportunities of using remote sensing-based methods that require large amounts of reference data for calibration and parametrization. For instance, Kolendo et al. (2021) used a large-scale reference dataset to parameterize ITD algorithms in coniferous forests, reaching tree count RMSEs varying from approximately 6 to 13%, depending on the forest type. Skudnik and Jevšenak (2022) found that, in the presence of sufficient reference data for calibration, artificial neural network-derived tree height predictions can outperform predictions derived from mixed effect models. Generally, deep learning methods require large datasets for calibration to be used at their full potential (Hamraz et al., 2019; Xi et al., 2020).

In addition, the type of reference data is a constraint while working with remote sensing-based environmental assessments, because some forest attributes are not easily measurable with manual methods. For instance, Zhen et al. (2016) pointed out the difficulty to acquire precise tree locations in field reference data as a disadvantage of individual tree detection approaches in forest inventories. Another example is the estimation of stem profiles, which requires either destructive methods or heavy machinery to be measured. In this sense, the car-mounted MLS has the potential to provide data of the type and amount required by different applications and pose as a suitable reference data collection component in remote sensing-based forest inventories.

A possible drawback of such a solution is that at the roadside, where there is usually less competition among individual trees, the trees are under edge effect and may show different growth rates and patterns compared to trees further into the stand (Delgado et al., 2007; Harper et al., 2015). Consequently, a car-mounted MLS solution that limits data collection to the roadside might sample mostly trees that are not representative of the whole forest and may not be suitable for calibrating remote sensing-based models.

The main objective of this study is to assess the suitability of a car-mounted MLS sensor to retrieve field reference data along forest roads. We assess the potential of such technology in providing reference data for remote sensing-based forest inventories. The specific objectives are: (1) to propose algorithms for ITD (Individual Tree Detection), DBH, stem profiles, and total volume estimation with MLS data, and (2) to assess the influence of distance from the roadside on the estimations.

## 2. Material and methods

### 2.1. Study area and reference data

The proposed algorithms were validated on the Remningstorp test site, in Southern Sweden (lat. 58.5 degreesN, long. 13.6 degreesE), where the dominant tree species were Norway spruce (*Picea abies*) – 85.7%, Scots pine (*Pinus sylvestris*) – 9.1%, and Birch (*Betula* spp.) – 3.4%, with density of 580 trees/ha. Altogether, 18 circular plots with a radius of 10 m were measured in the field during summer 2017. In each field plot, all living trees with a DBH greater than 4 cm had their DBH and position recorded. The mean DBH of the measured trees was 26.7 cm, with approximately 95% of all measured trees having DBH >= 15 cm. The plots were organized in six groups, with the plot centers aligned perpendicularly to the road (Fig. 1).

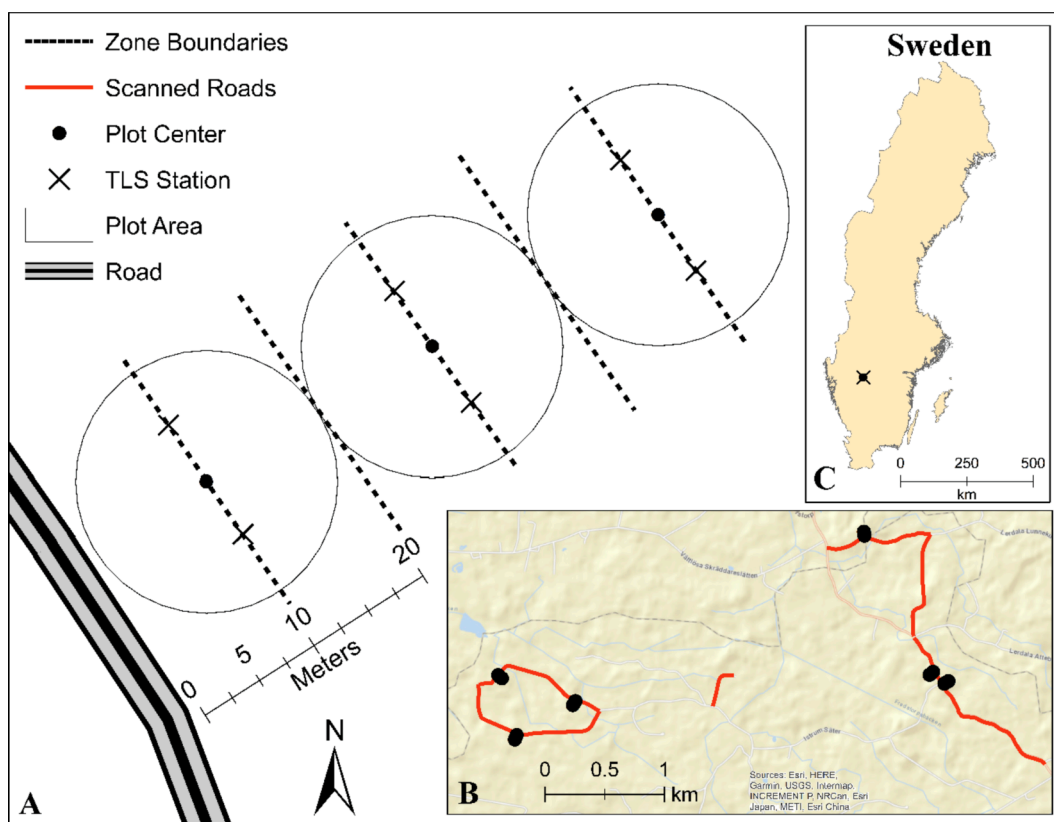To evaluate the effect of the distance from the road on the proposed

**Fig. 1.** Schematic representation of spatial disposition of a group of plots in relation to the roadside and TLS survey setup (A), with details of the position of the plots in the study area (B), and position of the field plots in Sweden (C).

method's accuracy, we divided the trees into 6 range zones, according to their distances from the roadside: 0–10 m, 10–20 m, 20–30 m, 30–40 m, 40–50 m, and 50–60 m (Fig. 1).

In November 2019, TLS surveys were conducted in each group using a multi-scan setup, with 2 scans per plot (Fig. 1). The TLS sensor used was a Trimble TX8. The wavelength was near-infrared (1500 nm) and repetition rate was 1 million points per second. The field of view was 360 degrees in the horizontal and 317 degrees in the vertical direction, and the point spacing of 0.4 cm at 10 m from the scanner. The footprint diameter was 3.4 cm at 100 m from the sensor. The system records up to three returns from the same pulse with a range accuracy less than 0.2 cm.

The TLS point cloud was processed according to Olofsson and Holmgren (2016). The stem volume was estimated for the TLS data using the stem curve procedure described in section 2.3.7. In comparison with field-measured DBHs, the TLS measurements had an overall Root Mean Squared Error (RMSE) and bias of 1.54 cm and 0.93 cm, respectively. Table 1 shows the RMSE of TLS-derived DBH estimates for each distance range from the road. These values are higher than the reported by Olofsson & Holmgren (2016) of 1 cm RMSE. This difference may be partly explained by the two years elapsed between the field and TLS

surveys, which might also have caused the systematic overestimation evidenced by the positive bias. In addition, zones as 0–10 m and 50–60 m were scanned by the TLS from only one direction, whereas the zones from 10 to 50 m had TLS positioned in both sides of the trees. This scanning set up might have caused lower accuracy in the closest and furthest distance ranges.

### 2.2. Mobile and Airborne laser scanning systems and Pre-processing

The MLS data survey was carried out using a car-mounted Riegl VUX-1LR sensor in November 2019. In total, approximately 7 km of forest roads were scanned in the both sides, yielding 84 ha of scanned forests considering the 0–60 m range. The car had a speed of 8 km/h and the sensor was leaning 30 degrees from the horizontal plane, with the side of the sensor pointing up and turned toward the front part of the car. The sensor shot near-infrared (1550 nm) pulses at a repetition rate of 820 Hz, which together with a field of view of 330 degrees yielded the angular step width (ASW) of 0.0066 degrees. The footprint diameter was 5 cm at 100 m from the sensor. The system records up to three returns from the same pulse with point registration accuracy of 1.5 cm.

The Airborne laser scanning (ALS) data was collected in October 2019 with a Leica TerrainMapper-LN system from approximately 1450 m above ground. The airplane had an average speed of 115 knots. The laser beam footprint was 0.35 m, the pulse frequency equal to 1600 Hz, and the scanner field of view equal to 30 degrees. The average point density was approximately 22 points/m$^2$.

Before ITD, the point clouds were classified into ground and non-ground points using the ground classification algorithm by Zhang et al. (2016) implemented in the lidR R package (Roussel et al., 2020). Once classified, we divided the MLS point clouds in two. The first point cloud excluded the ground points, and this was used for ITD, diameter, and stem profile estimation. The second point cloud was formed by only

**Table 1**
RMSE and bias of TLS-derived DBH estimates according to the distance range from the road.

| Zone | RMSE | Bias |
|------|------|------|
| 0–10 m | 2.57 cm (10.7%) | 2.35 cm (9.87%) |
| 10–20 m | 1.53 cm (5.60%) | 1.04 cm (3.81%) |
| 20–30 m | 1.40 cm (5.06%) | 1.11 cm (4.02%) |
| 30–40 m | 1.55 cm (5.62%) | 0.85 cm (3.11%) |
| 40–50 m | 1.32 cm (5.15%) | 1.01 cm (3.94%) |
| 50–60 m | 1.62 cm (6.36%) | 0.82 cm (3.22%) |

the ground points and used to find the aboveground height of the trees.

### 2.3. Individual tree Detection, stem Profiling, and stem curve estimation

The scanner's setup was chosen to facilitate tree detection and stem diameter estimation. The sensor's high repetition rate, combined with a scanning frequency lower than that normally used in surveys, yielded point clouds with high density within scan lines, but two consecutive scan lines are more separated in space. For instance, at 40 m from the sensor, two consecutive points were approximately 0.5 cm apart, whereas two consecutive scan lines were approximately 17 cm apart. The scanning frequency was chosen to yield very high density in stem cross sections, facilitating branch filtering and circle fits. However, it caused a significant loss of information in the vertical direction along the stem. Thus, this setup provided a better representation of the the targets in the scanline direction than in three dimensions, since solid targets—like stems—do not become represented in the point cloud as continuous surfaces, but rather as a collection of cross sections (Fig. 2). For this reason, the proposed ITD algorithm assumed that points belonging to the same stem appear in the point cloud as arcs, and it finds point clusters with circular shape within each scan line. After that, the identified arcs were segmented into single stems. Next, to estimate the stem profile, we divided the detected stems into sections, corrected their inclination (to point straight up), and estimated their diameter.

One characteristic of the car-mounted MLS data is the uneven point density of the point cloud (Fig. 3), which varied according to the distance from the sensor: while areas closer to the road (and thus closer to the sensor) had trees with both the stem and canopy scanned, trees further into the stand might have lacked several portions of the stem and
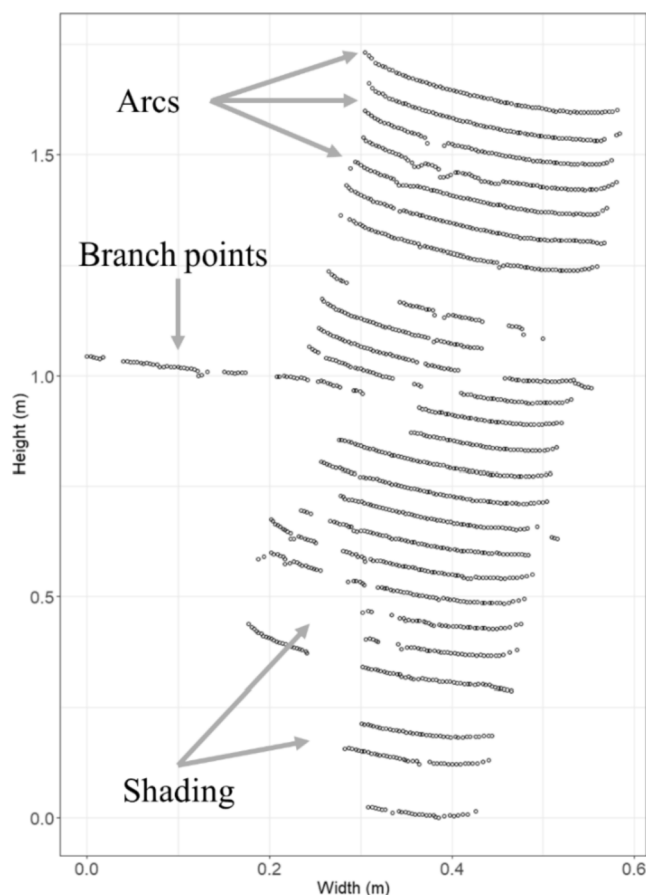


**Fig. 2.** Representation of a stem section in the car-mounted MLS point cloud. The stem is represented as a collection of arcs. It is possible to notice branches and shaded areas.

did not have returns from the upper canopy part, which prevented the retrieval of total heights from the MLS point cloud for many trees in these areas. To contour this issue, each tree's total height was retrieved from ALS instead of MLS point clouds. Total heights can also be modelled based on other tree attributes, however, in this study we used ALS-retrieved values in order to better understand the effects of the distance from the road in the estimates.

Finally, once the stem profiles of each tree were estimated, a stem curve model was fit to each detected tree. With such model, we could estimate diameters at any height of the tree even though it might not have been scanned. A flow chart of the method is presented in Fig. 4, and the details of each step are described in the following sections.

#### 2.3.1. Intensity-based point clustering per scanline

The trees were independently detected in each scanline by finding arcs in the point cloud, as in Forsman et al. (2016). In this step, we assumed that points close enough to each other could be considered as returns from the same target, e.g., the same stem.

The algorithm operates in each scanline in two steps. First, it clusters points together and secondly, it uses intensity thresholds to select only reliable laser returns in each cluster. This avoided inaccurate echoes at the edge of the stem due to, for instance, the laser beam's footprint (Forsman et al., 2018, 2016). This process works as follows:.

- For each scan line, cluster together points that are at a maximum distance $d_t$ cm from each other. In other words, inside a cluster a point should be maximum dt cm from its nearest neighbor in the same cluster. The cluster should have at least 15 points;
- For each cluster, save the 95th intensity percentile as the intensity peak *(Ip)*. Then filter out points with intensity value less than 70% of *Ip*.

The threshold distance $d_t$ used to cluster points together was based on the laser survey's angular step width (*ASW*) and accuracy (*A*). It denotes the maximum distance a point in a given cluster should be from its closest point in the same cluster. It is given by equation (1),

$$d_t = \sin(ASW/2)*D*2 + 2*A, \tag{1}$$

where the first part of the equation denotes the minimum distance between two consecutive points at a given distance *D* from the sensor, assuming the points have reflected from a perfectly flat target. The ASW represents the angular separation between two consecutive laser pulses. Finally, different factors, such as the stem shape and point positioning errors, could cause the distance between two consecutive points to be bigger than the theoretical one. For this reason, we added two times *A* to $d_{min}$ to form $d_t$, accounting thus for both the circular shape of the stem and inaccuracies in the point's position.

#### 2.3.2. Circle fitting

The first circle fitting was done for two reasons: first, to eliminate point clusters that do not have the arc shape we assume stems to have, and second, to obtain coordinates for each circular cluster, which will be subsequently used to segment the arcs into tree stems.

To fit the circle, we used the modified version of the Random Sample Consensus (RANSAC) algorithm described by Olofsson et al. (2014). This algorithm iteratively fits circles to a given set of points and chooses the best fit (Fig. 5). The circles were fit to the projection of the points on the horizontal plane, i.e., only the X and Y coordinates were used in the fitting process. The number of iterations for each cluster was set to 140, based on the probability of finding a good circle model, as in the paper by Olofsson et al. (2014). In each iteration for a given cluster, three points were randomly selected and a circle was fit to them. For each iteration, we recorded the number of inliers as being the number of points within a given tolerance distance from the circle. The points outside this tolerance distance were considered outliers. Each iteration determines unique sets of inliers and outliers, which are not dependent
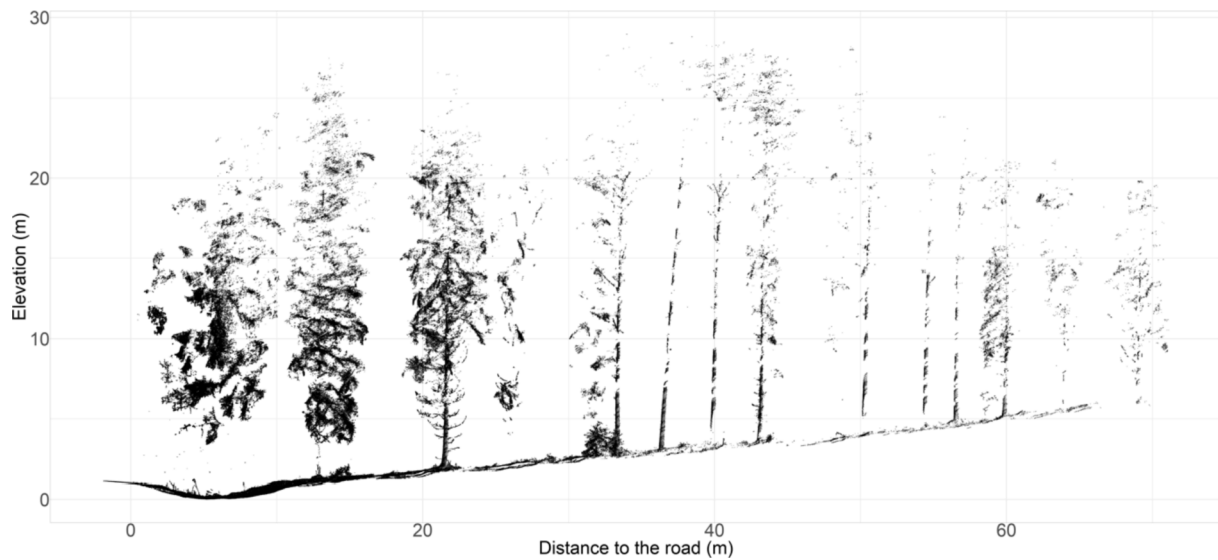
**Fig. 3.** Representation of 3D point cloud, where the point density varies according to the distance from the sensor. The left side is closer to the sensor than the right side and has more points in the canopy and on the stem compared to the trees in the right side of the figure.
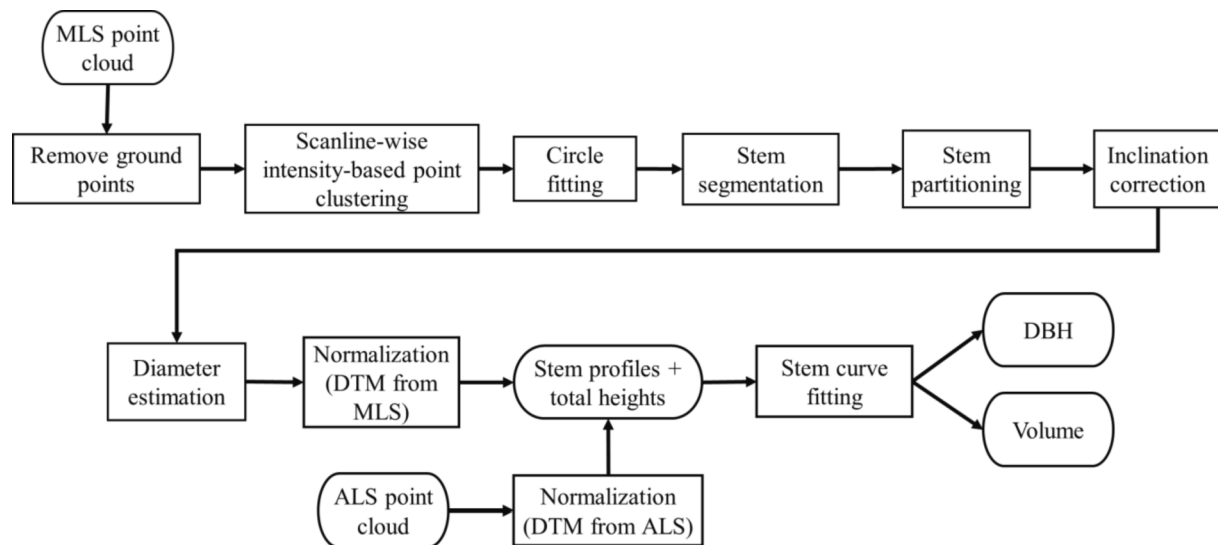


**Fig. 4.** Flowchart showing the processing of MLS point cloud.

on the other iterations. In this study, we decided to set this tolerance distance equal to the accuracy of the laser survey, which was 1.5 cm.

We assumed that the laser beam cannot go through the stem, so if the randomly chosen circle in a given iteration had more than 1% of the outliers inside the trunk, the iteration was considered invalid. Then, we selected the fit with the highest number of inliers amongst the valid iterations as the best fit. After the best fit is selected, the outcomes of all the other iterations are ignored. The inliers of the best fit were used in a final adjustment by iteratively looking for the circle with smallest mean squared distance between its inliers and its edge. The center coordinates (X, Y), its radius and height (median height of the points), were recorded for the next step.

*2.3.3. Stem segmentation*

Since the trees were detected independently in each scan line, it was necessary to vertically aggregate the arcs to build consecutive tree stems. Thus, in the stem segmentation, we associated several arcs to a single stem using the circle center locations obtained in the previous step, according to the tree stem segmentation proposed by Holmgren et al. (2019):

- For each arc's circle, estimate a direction vector ($Vd_i$) using other circles within a 50 cm radius of the target circle with Principal Component Analysis (PCA). Use the center coordinates (X, Y and height) of the circles as input;
- For each $Vd_i$, calculate the root-mean-square-deviation (RMSD) of the 3D linear distance of the circles' centers to $Vd_i$;
- Sort all the *Vds* from the smallest to the largest RMSD;
- For each $Vd_i$, starting from that with smallest RMSD, segment to the same stem all the arcs whose circular areas – generated in section 2.3.2 – are crossed by $Vd_i$. In other words, segment to the same stem all circles crossed by the direction vector calculated in the first step. Repeat this step until no more arcs are available (i.e., no more arcs without a stem associated).

Once the arcs were segmented into stems, we recorded the position of the lowest arc as the position of the stem.
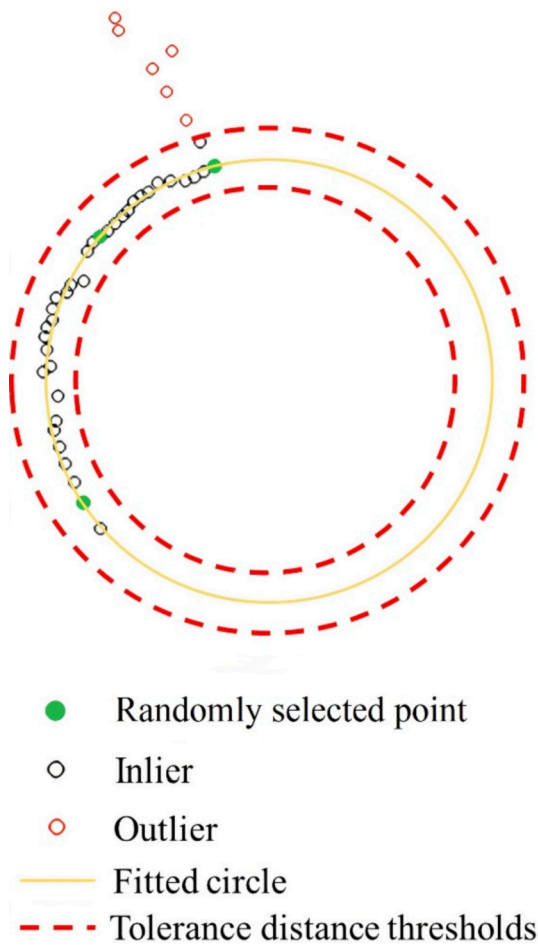
**Fig. 5.** Schematic representation of the point selection done by the modified RANSAC (Olofsson et al., 2014).

### 2.3.4. Stem partitioning

Neighboring arcs from the same stem were grouped to provide better input data for the circle fitting than would be possible using a single arc (Fig. 6 A and B). This process, which we called stem partitioning, was necessary for two reasons. First, branch points are often classified as stems, especially in transition areas where both connect. Second, the identified arcs might have imperfections, such as gaps or noise around them (Fig. 2).

The grouping was done by partitioning the segmented stem into small sections of 30 to 50 cm. The size of the section was dependent on how many arcs could be found in each height interval. In this study, the minimum number of arcs in each section was defined according to the laser survey's setup, which gives that two consecutive scan lines would be 17.1 cm apart from each other in height. Thus, on a 30 cm long section of a given stem, we expect to find two arcs. However, this distance between scan lines can vary according to the car's speed during the survey. Hence, when fewer than two arcs were found in a 30 cm section, the section size was increased by 10 cm until it reached 50 cm, or until the minimum of two arcs were found. If at least two arcs were not found in a 50 cm interval, this interval was considered empty and not used in the stem profiling. In the first two zones, from 0 to 10 m and 10–20 m, we recorded stems with at least 10 sections, to avoid classifying bushes or branches as trees. When stems in those zones had fewer than 10 sections, they were considered noise.

### 2.3.5. Inclination correction

Hyyppä et al. (2020b) demonstrated that the horizontal projection of points from inclined stems can lead to biased diameter estimations when trees lean more than 3–4 degrees. To avoid such errors, stem direction should always be perpendicular to the plane on which the points are projected.

In this study, diameters were always estimated in the horizontal plane. Therefore, the stem's inclination was corrected before projecting its sections. It is also important to note that a stem's inclination is not constant along the tree. For this reason, we corrected the inclination at each 2 m of stem, respecting the sections defined in the previous step: we found the direction vector of each 2-meter log simply by getting the centroids of the log's upper- and lowermost sections. Then, we rotated
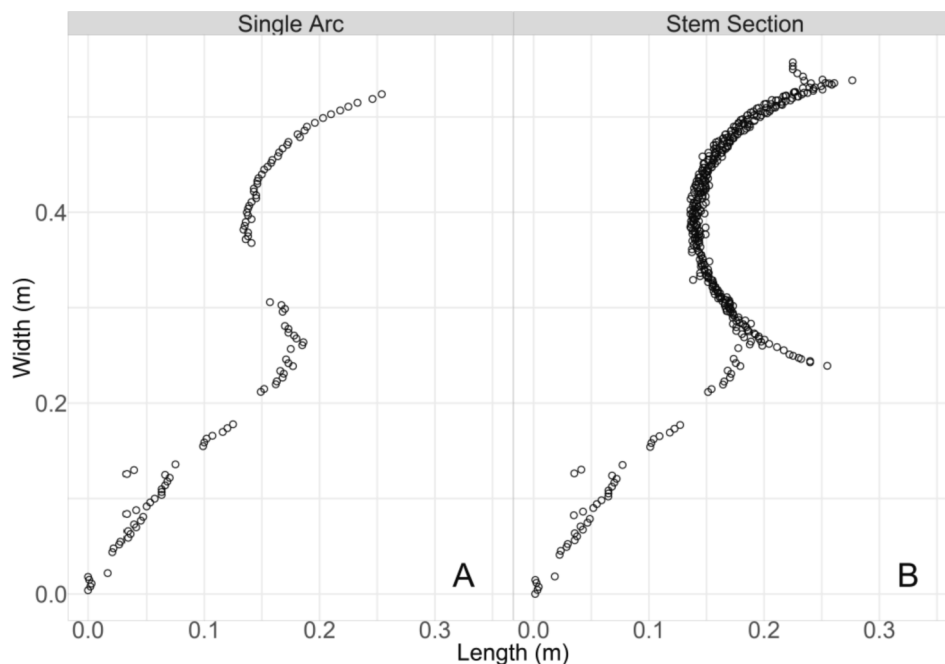


**Fig. 6.** Representation of a stem section from a Norway spruce tree where all points were classified as stem points. A: Single arc seen from above; B: group of arcs (stem section) seen from above.

the log to match a vector of the same size with its upper- and lowermost sections vertically aligned.

### 2.3.6. Diameter estimation

After defining the sections and correcting their inclination, we estimated the sections' diameters by fitting circles to the projection of each section's points on the horizontal plane. The main difference between the two circle fit steps in this study is that in section 2.3.2 the process was done at arc level (i.e., only one scan line), whereas in the current step the fit was done at section level (i.e., group of arcs).

In addition, the circle fit for diameter estimation was done in two stages as proposed by Lindberg et al. (2012), making the estimation less sensitive to the local influence of branches. In the first stage, we fitted circles as described by Olofsson et al. (2014). In the second stage, the center positions $(X_c, Y_c)$ and diameters (D) from the circles in the first stage were used to select a new set of points. If we let $(x_i, y_i)$ be a point coordinate from the stem section we are analyzing, we select the points that meet the criteria in equation (3) in the second stage.

$$(X_c - x_i)^2 + (Y_c - y_i)^2 \leq (p*D/2)^2 \tag{2}$$

where $p$ is a constant that expresses the maximum distance from the circle center $(X_c, Y_c)$ a point $(x_i, y_i)$ should be so it would be included in the second stage, expressed as a proportion of the radius value found in the first stage. In this study, we use $p = 1.1$.

At last, a final circle fitting was done using the points selected in the second stage, and the diameter value and section height found were recorded as the stem profile of the tree.

### 2.3.7. Stem curve

We used the stem curve model by Hyyppä et al. (2020b) to describe the diameter variation along a tree's stem, estimating diameter values for regions of the tree that have not been scanned, e.g., the treetop and DBH height. The model combines equations (4) and (5).

$$R_a(z) = a_1*(H - z) + a_2*(H - z)^2, \tag{3}$$

$$R_b(z) = b*\sqrt{(H - z)}, \tag{4}$$

where $H$ is the total height of the tree retrieved from ALS, and $R(z)$ is the radius at the height $z$. Both $a_1$, $a_2$, and $b$ are coefficients to be determined with least square regression. With the coefficients, equation (5) gives the stem volume (V).

$$V = \pi \bigg/ 2* \left( \int_0^H R_a(z)^2 dz + \int_0^H R_b(z)^2 dz \right). \tag{5}$$

The system composed by equations (3) and (4) was chosen for several reasons, as pointed by Hyyppä et al. (2020b). First, the small number of coefficients used in the equations make the model robust to deal with outliers along the stem profile. Second, the average of both equations (effective fit) fits well to the stem profile, performing similarly in trees with several diameter values measures along the stem (Fig. 7 – Tree A), and trees with less measurements (Fig. 7 – Tree B).

To obtain accurate total heights for all the trees we use ALS data over the same area. The retrieval of total heights from the ALS point cloud was done with a 30 cm radius search around the MLS-retrieved tree positions. Inside this radius, the highest height value was considered the tree's total height.

### 2.4. Accuracy assessment

Different reference data sources were used to assess the accuracy of the variables retrieved with the car-mounted MLS. The accuracy of the ITD was assessed in each zone by matching the MLS-detected trees with the field-recorded tree positions. This was done by conducting a radius search around 30 cm of each MLS-detected tree. If an MLS-detected tree corresponded to a field-recorded one, the tree was considered a true positive. If it did not correspond to any field-recorded tree, it was considered a commission error. Finally, we considered omission when a field-recorded tree position did not have any correspondence with the MLS-detected individuals. Then, we computed the precision (equation (6)) and sensitivity (equation (7)) to quantify the accuracy of the ITD:

$$Precision = TP/DT, \tag{6}$$

$$Sensitivity = TP/(DT + OT), \tag{7}$$

where TP is the number of trees correctly detected (true positives), DT is the total number of trees found by the proposed ITD algorithm, and OT is the number of trees present in the reference data which were not found by the proposed method (omissions).
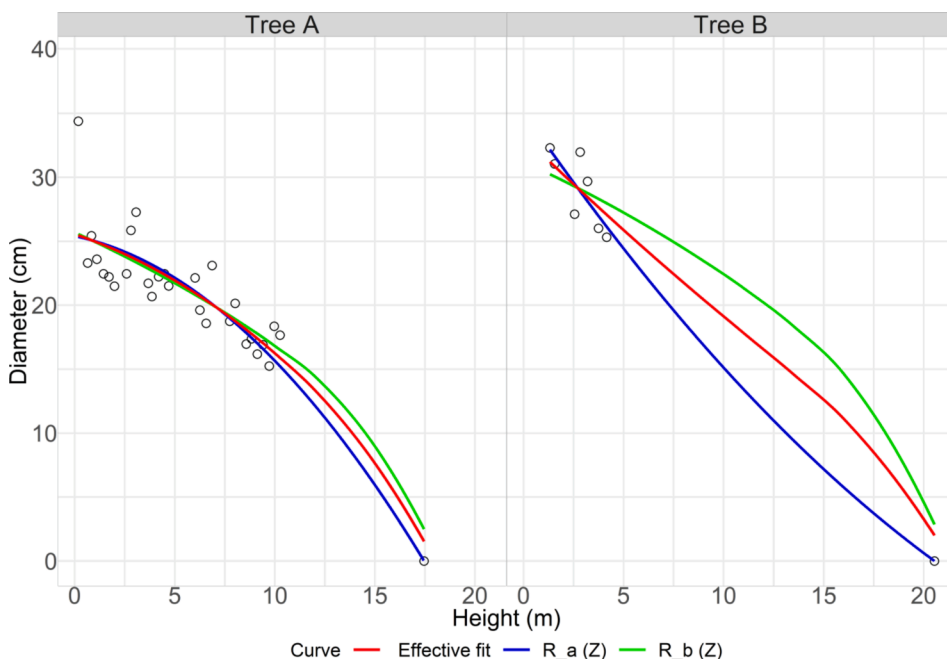


**Fig. 7.** Parabolic function $R_a(z)$ in blue (equation (3)), square root function $R_b(z)$ in green (equation (4)) that compose the stem curve model fit to the stem profiles of two different trees (Tree A and B). The average (effective fit) of $R_a(z)$ and $R_b(z)$, which is used to estimate the effective diameter values and stem volume, is shown in red. Trees A and B have different number of diameter measurements along the stem. (For interpretation of the references to colour in this figure legend, the reader is referred to the web version of this article.)

TLS-derived DBHs, stem profiles and total volumes were used as reference to assess the accuracy of MLS-derived estimates of these three forest attributes. In this study, TLS-derived values were preferred over other methods of reference data collection once the measurement of stem profiles and volume though destructive methods was not feasible. Thus, in each zone, the performance of the proposed method was evaluated by comparing the MLS-derived and TLS-derived DBHs, stem profiles and total volumes of each detected tree by computing the RMSE - equation (8) - and bias - equation (9). The relative RMSE and bias were calculated in relation to the reference mean values of each variable.

$$RMSE = \sqrt{\sum_{i=1}^{N} (\widehat{y}_i - y_i)^2 \bigg/ n}, \tag{8}$$

$$bias = \sum_{i=1}^{N} (\widehat{y}_i - y_i) \bigg/ n, \tag{9}$$

where $y_i$ and $\widehat{y}_i$ are the target's variable reference and estimated values, respectively, for unit $i$ and $n$ is the total number of units.

To compare the stem profiles obtained with the two methods, we defined a comparison range that comprehends the height interval of the stem where both MLS and TLS measurements are available. Inside the comparison range, we calculated the average diameter for each 1-meter interval, thus reducing the local influence of outliers in both the MLS and reference datasets.

Finally, we evaluated the difference of the diameter distributions obtained with the different sensors in each detection zone (5 cm classes). For that, we used the error index $e$ (Reynolds et al., 1988) proposed by Packalén and Maltamo (2008), as in equation (10),

$$e = \sum_{i=1}^{N} 0.5 \times |f_i/N - \widehat{f}_i/\widehat{N}|, \tag{10}$$

where $f_i$ and $\widehat{f}_i$ are the number reference and MLS-detected trees in diameter class $i$, respectively. $N$ and $\widehat{N}$ are the total number of reference and MLS-detected trees, respectively.

## 3. Results

### 3.1. Individual tree detection

Table 2 shows a summary of ITD's precision and sensitivity in different zones. The ITD performance varied according to the tree's distance from the road. From 0 to 10 m, we noticed the lowest precision and sensitivity in the study. This is mostly due to the high number of large branches and the proximity to the sensor. From 0 to 10 m from the road, we observed bigger branches compared to areas further into the stand. This factor, combined with the proximity to the sensor, meant that such branches were heavily scanned, causing some of them to be classified as separate trees (commission errors). At the same time, omission errors were caused by the high proportion of branches in the trees in this zone, which made discriminating between branches and stems not always possible. For instance, some stems might have been visible but could not be considered circular due to the amount of noise

around them. In these cases, the stems were filtered out of the point cloud.

The ITD had the best performance in the intermediate zones. Similar figures were observed from 10 to 20 m, 20–30 m, and 30–40 m, with both precision and sensitivity exceeding 90%. In these zones, the branches are smaller compared to the first zone, which made discriminating between branches and stems easier. Besides, in the intermediate zones, the point density is not as high as at 0–10 m from the road, causing fewer commission errors.

Beyond 40 m from the roadside, as distance to the sensor increases, we observe high precision and decreasing sensitivity. In these zones, few or no commission errors were observed, which justified the high precision values. However, as trees get more distant, the chances of occlusion increase and point density decreases, making it more likely that fewer points would hit the stems, and thus more difficult to discriminate between stem and crown.

### 3.2. DBH, stem profile, and DBH distributions

The prediction accuracy of DBH varied through the different zones (Fig. 8), with the RMSE and bias ranging from 1.81 cm (6.38%) to 4.84 cm (16.9%), and −0.41 cm (-1.35%) to 0.82 cm (2.86%), respectively. In some zones, e.g., from 0 to 10 m, the presence of outliers and the lower accuracy of the reference data in this zone influenced the accuracy of the predictions more. However, most errors were between ± 10%. In addition, the variation of RMSE in the different zones is a consequence of the presence or absence of scan arcs around the DBH height (1.3 m). Some trees do not have arcs near 1.3 m, which causes their DBH values to be a result of the stem curve built from diameter values at higher parts of the tree and creates the observed outliers.

The stem profile estimates (Fig. 9) had slightly lower RMSE than the DBH estimates, ranging from 1.58 cm (6.26 %) to 2.18 cm (8.76%). The bias ranged from −0.44 cm (-1.58%) to 0.22 cm (0.84%). We assessed the accuracy only in the scanned regions of the stem (comparison range), so these error values concern only the stem regions with both MLS and TLS data. On the other hand, DBH estimates were retrieved from a stem curve model, since not all the trees were scanned at 1.3 m height. For this reason, the DBH-related accuracy contains not only errors from the stem profiling, but also errors from stem curve fitting.
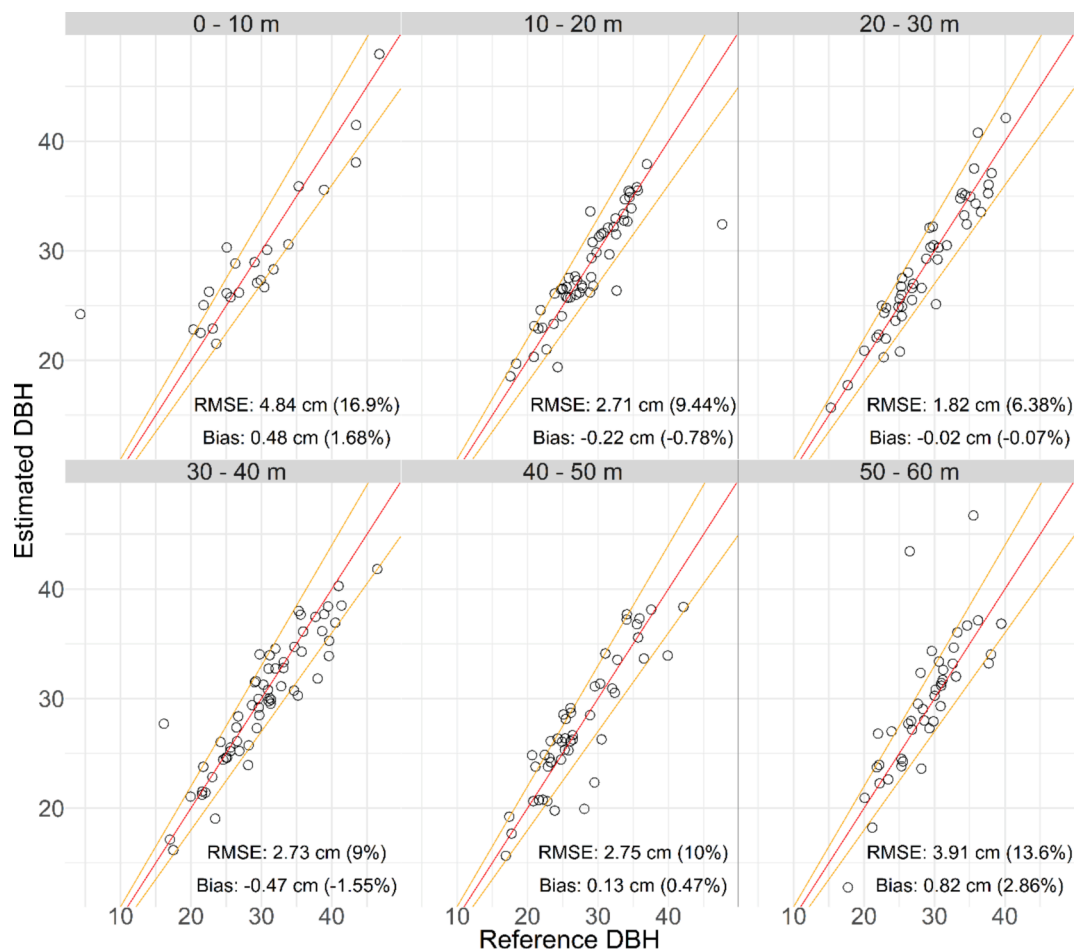
The error index of diameter distributions ranged from 0.11 to 0.33 (Fig. 10), with no trees below 10 cm DBH being correctly estimated, regardless of the zone. However, our study area had a few small trees (DBH < 10 cm), which does not allow a proper evaluation of the estimations in this stratum. The largest $e$ was observed from 0 to 10 m. The smallest $e$ values were found from 30 to 60 m, where $e$ was equal to 0.11.

### 3.3. Volume

The stem volume estimates had the highest relative RMSEs in this study, ranging from 0.08 m³ (10.1%) to 0.19 m³ (25.7%) and bias from −0.03 m³ (-4.07%) to 0.19 m³ (8.25%) (Fig. 11). The highest RMSE and bias are in the first zone (0–10 m). The stem volumes are more likely to be overestimated in the zones closer to the road, whereas values further into the stand tend to be systematically underestimated.

We also compared the total reference and estimated total volumes of each zone (Table 3). For these estimates, the accuracy was highly correlated with the ITD performance in each zone, with the volume of omitted or commissioned trees being the main error source. For instance, both commission errors and the systematic overestimation of stem volumes observed from 0 to 10 m caused the total volume for the zone to be overestimated by 13% in average. On the other hand, omissions might have caused the underestimation observed from 50 to 60 m, where 66.6% of the total reference volume was detected. The area-level estimates performed better in the intermediate zones, where the ITD had the best overall performance. In the intermediate zones, the mostly small trees are omitted, which did not seem to influence the total volume

**Table 2**
Individual tree detection (ITD) precision and sensitivity according to the distance range from the road.

| Zone | Precision | Sensitivity |
|---|---|---|
| 0–10 m | 82.8% | 85.7% |
| 10–20 m | 96.5% | 96.7% |
| 20–30 m | 98.8% | 94.2% |
| 30–40 m | 92.5% | 92.5% |
| 40–50 m | 98.0% | 86.1% |
| 50–60 m | 100.0% | 62.7% |

**Fig. 8.** Reference vs. estimated DBH. The red line is the 1:1 line, where reference and estimated values are equal. The orange lines represent a 10% deviation from the 1:1 line. RMSE = Root Mean Square Error. (For interpretation of the references to colour in this figure legend, the reader is referred to the web version of this article.)

estimates.

## 4. Discussion

### 4.1. Algorithm performance

The sensor configuration was tailored to detect tree stems along forest roads. Its high repetition rate combined with the sensor's inclination provided detailed cross sections of stems and enabled collection of data from both the ground and upper canopy. In this study, we proposed an algorithm for individual tree detection designed for such a sensor configuration, identifying the cross sections (or arcs) in the point cloud and aggregating those into single trees.

ITD is the key task in many MLS applications and is often the first result reported in several studies. The ITD method we proposed had a performance in the zones from 10 to 40 m (Table 2) comparable with that of other state-of-the-art methods: Liu et al. (2021) reported 96.7% precision and 93.5% sensitivity in a natural forest site with approximately 411 trees per hectare. Different precisions and sensitivities were found in the benchmark study by Hyyppä et al. (2020c), depending on the type of forest and MLS sensor. In obstructed forest (approximately 420 stems/hectare), the authors reported precisions and sensitivities of 100% and 79% respectively with backpack MLS, 100% and 76.7% with hand-held MLS, and 100% and 81.4% with under-canopy ULS. In sparse forest plots, with around 410 stems/hectare, the ITD performed better. Under these conditions, precisions and sensitivities of 100% and 92.9% respectively were found with all three systems, the backpack and hand-

held MLSs and the under-canopy ULS. In these studies, the sensors were moving inside the forest plot, with a maximum distance from tree to the closest sensor of 20 m. In our study, depending on the zone, trees could be up to 60 m from the closest sensor location, which explains the lower ITD accuracy in zones far from the road.

The accuracy of DBH estimates (Fig. 8) achieved with our method ranged from 1.82 cm (6.38%) to 4.84 cm (16.9%) in the different zones. These estimates were less sensitive to the distance from the road, which made it possible to obtain accurate DBH estimates in all six zones. Our results are in-line with accuracies reported by other authors with different vehicle-mounted MLS systems. For instance, Bienert et al. (2018) used a highly accurate car-mounted MLS to estimate DBH with 3.7 cm RMSE, using field-measured DBHs as references. In addition, Liang et al. (2018b) reported an RMSE of 11.2% in DBH predictions with ATV-mounted MLS in boreal forests with approximately 600 stems/ha. Finally, Pierzchała et al. (2018) used a ATV-mounted MLS system composed by a Velodyne VLP-16 sensor, a stereo camera, an IMU, and a GPS to measure DBHs with RMSE equal to 2.4 cm.

The lowest RMSE in DBH estimation was found at 20–30 m from the road, a zone where we did not observe any outliers, which implies that the accuracies in the other zones could potentially be improved by using refined methods of outlier correction and different sensor set-up. For instance, a more efficient branch filtering method could improve not only the accuracy of DBH estimates but also tree detection, e.g. in zones where the large amount of unfiltered branches prevent the stems from being detected due to the algorithm's inability to identify circles in such cases. In addition, a reduced gap between two consecutive scan lines
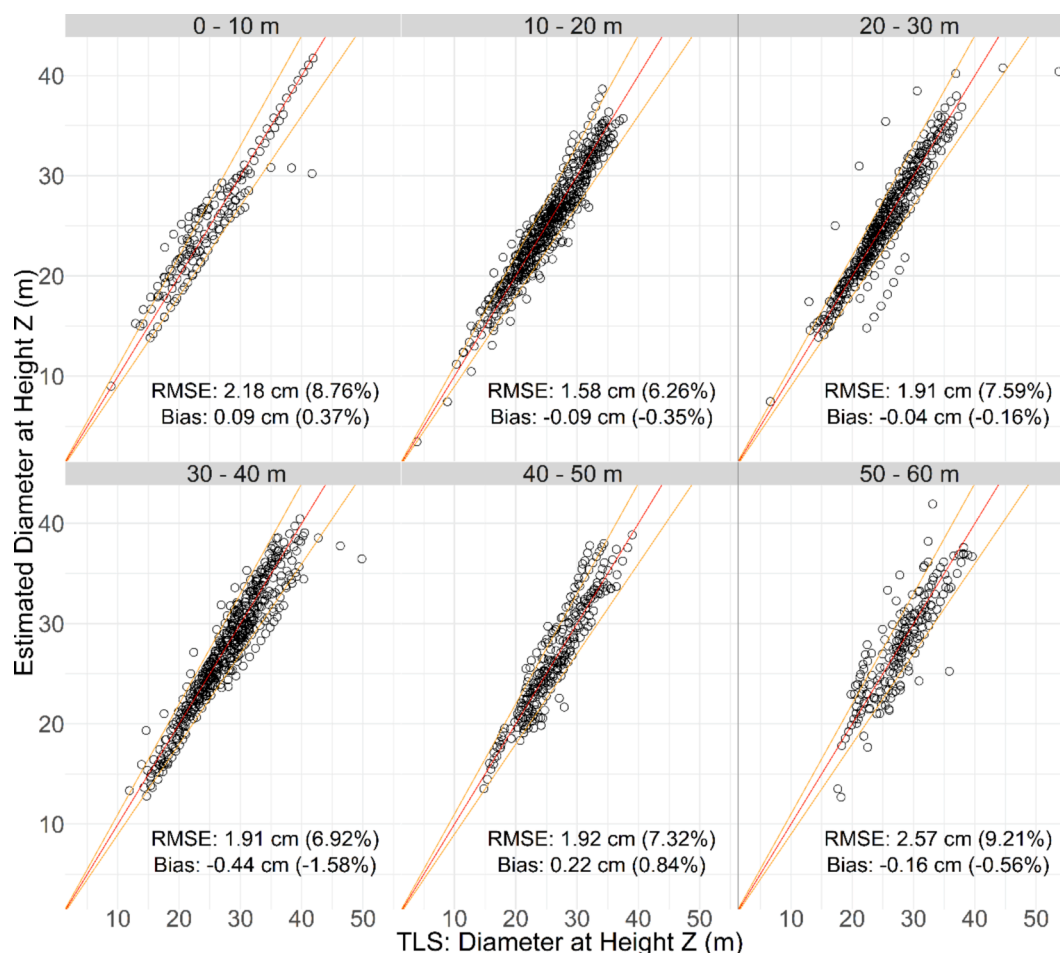
**Fig. 9.** Reference (TLS) vs. estimated (MLS) stem profile. The red line is the 1:1 line, where reference and estimated values are equal. The orange lines represent a 10% deviation from the 1:1 line. (For interpretation of the references to colour in this figure legend, the reader is referred to the web version of this article.)

could increase the amount of diameter measurements along the stem and the chances of having a measurement around 1.3 m, which would make both DBH and stem volume estimates more accurate regardless of the zone.

*e* is a measure of disparity between two distributions generated with different methods. In our study, the variation in *e* could be partially explained by the DBH estimates' error: tree-level errors caused stems to be allocated in the wrong diameter classes, thus increasing *e* when comparing the estimated and reference DBH distributions. For instance, in our study the highest *e* (0.33) was found in the 0–10 m zone, with one of the highest RMSEs (4.84 cm) and biases in DBH estimation (0.48 cm).

Stem profiles describe stems' shape and can be used to calculate stem volume. However, a manual diameter measurement of the higher part of the stem is impractical in operational forest inventory, since the trees would need to be felled before the measurements are conducted. Therefore, different TLS and MLS solutions have been proposed as non-destructive and efficient alternatives to stem profile measurement, and the method we describe in this study provided stem profiles with comparable accuracies (Fig. 9). For instance, a benchmark study by Liang et al. (2018a) found RMSEs of stem curve estimation ranging from 0.9 cm to 5.0 cm when comparing 13 multi-scan TLS-based algorithms under different forest conditions. Hunčaga et al. (2020) compared the accuracies of stem profiles obtained with different sensors, finding RMSEs equal to 1 cm, 1.3 cm and 1.9 cm in stem profiles obtained with TLS, hand-held MLS and close-rage photogrammetric point clouds, respectively. In addition, Hyyppä et al. (2020a) assessed the accuracy of stem curves obtained with under-canopy ULS, reaching RMSEs equal to 1.2 cm and 1.4 cm in sparse and obstructed forest plots, respectively.

Finally, MLS-derived stem profiles can also be obtained with RMSEs ranging from 5.0% to 18.7% (Hyyppä et al., 2020b; Liang et al., 2018b) depending on, among other things, the type of MLS system and forest.

A drawback of the proposed method is that the stem profiles it provided were limited to the detectable portion of a tree's stem. In other words, even though we could obtain accurate estimates of the stem diameters at different heights regardless of the tree's distance from the road, the number of detected stem sections varied amongst trees, in our study ranging from a few units to tens. A challenge of working with largely varying stem profiles is finding a model capable of describing the stem curve accurately regardless of the number of available sections. To overcome this challenge, we used stem curve equations by Hyyppä et al. (2020b) (equations (3) and (4)), which were robust with both numerous and few stem profile measurements due to the low number of parameters to be calculated, thus preventing overfitting in stem profiles with only a few sections.

The accuracy of the stem volume estimates in our study varied from $0.08 \, \mathrm{m}^3$ (10.6%) to $0.12 \, \mathrm{m}^3$ (15.9%) in most of the zones, except at 0–10 m, where the RMSE was $0.20 \, \mathrm{m}^3$ (32.0%). The higher RMSE at 0–10 m can be at least partially explained by the lower accuracy of the reference in the same zone (Table 1). The bias of stem volume was mostly related to the distance from the road, varying from $-0.03 \, \mathrm{m}^3$ (-3.25%), at 30–40 m, to $0.06 \, \mathrm{m}^3$ (10.2%), at 0–10 m. Closer to the road (e.g. 0–10 m), branches were often classified as stem points, which caused them to be included in the circle fitting and diameter estimation procedures. For this reason, the stem volumes closer to the road were systematically over estimated (Fig. 11). Further from the road (e.g., at 50–60 m) the systematic underestimation was often due to the few sections used to
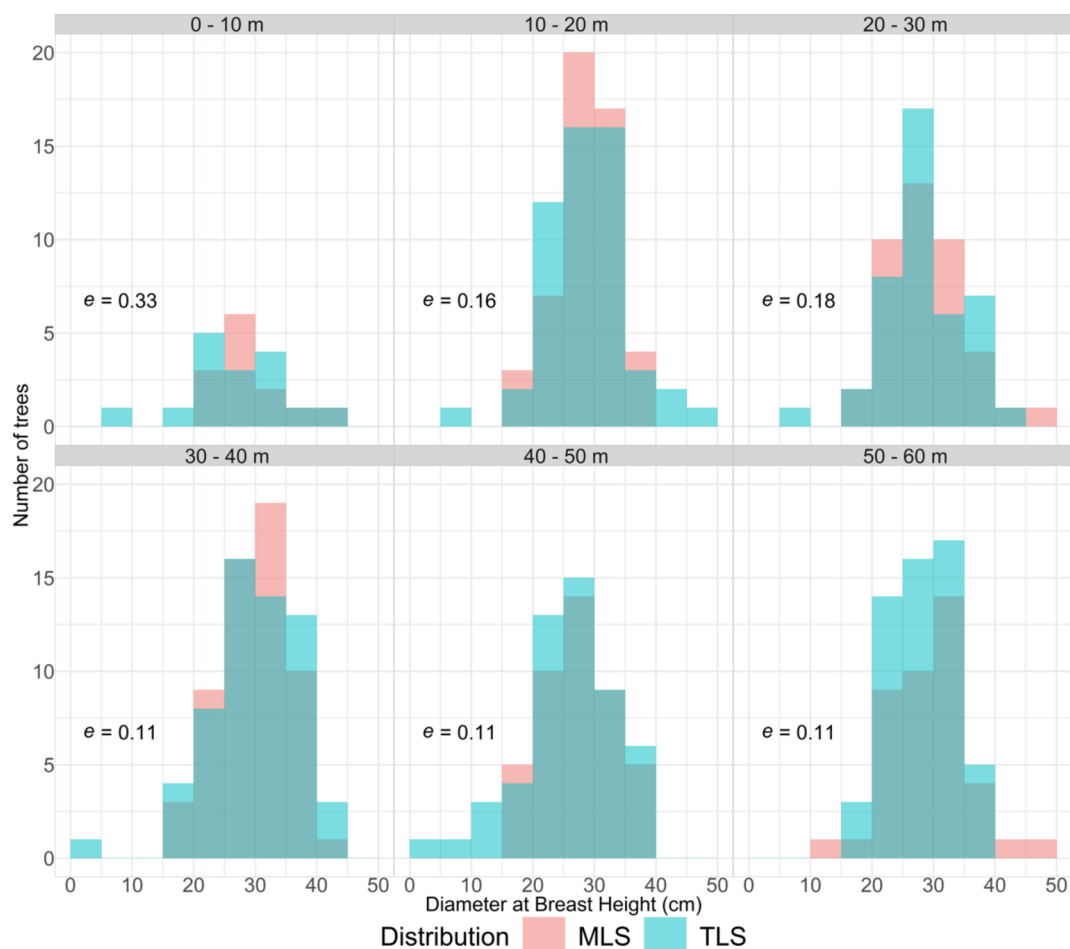
**Fig. 10.** DBH distributions and error index according to the distance from the roadside obtained with MLS (pink) and TLS (cyan), with overlaps in dark cyan. (For interpretation of the references to colour in this figure legend, the reader is referred to the web version of this article.)

estimate the stem curves in these areas. In other words, further from the sensor, the stem profiles may not represent the whole stem accurately and therefore lead to the observed underestimation.

Despite higher error at 0–10 m, our method performed in-line with other state-of-the-art methods for stem volume estimation. For instance, Hyyppä et al. (2020c) estimated stem volumes with relative RMSE ranging from 10% to 15% while benchmarking backpack and handheld MLS and depending on the MLS system used. Second, Liang et al. (2018a) reported relative RMSEs of volume estimates varying from 16.7% to 60.4% with different TLS-based algorithms in multi-scan setups. Third, Bienert et al. (2018) used car-mounted MLS to estimate, among other variables, merchantable and total stem volumes, reporting RMSEs equal to 0.4 m$^3$ and 0.6 m$^3$, respectively. Finally, the benchmark study by Liang et al. (2018a) compared different TLS systems and presented average RMSEs of 0.12 m$^3$, 0.21 m$^3$ and 0.18 m$^3$, in the easy, medium and difficult plots, respectively,.

Regarding total volume estimates, the RMSE (Table 3) ranged from 7.97% to 10.5% in most zones, except for the first and last zones, where commission and omission errors caused over and under estimations, respectively. These values are comparable with the accuracy of different LiDAR-based methods at the area level. For instance, Puliti et al. (2020) found a deviance of 32.2% at the plot level, 28.9% at the stand level, and 3.5% at the forest level when comparing under-canopy ULS- and field-based volume estimates. Maltamo et al. (2019) used accurate tree position data from harvester and ALS-based metrics to train k-NN (k nearest neighbor) estimators of total volume, reaching 9% RMSE in stand-level validations. Finally, Liang et al. (2018a) reported an average of 94% of total volume being detected with different TLS-based

algorithms.

### 4.2. Applicability

One advantage of using car-mounted MLS instead of other ground-based LiDAR systems is the data collection efficiency provided by the car-mounted platform and the forest roads. The MLS survey used in this study took 2 h, scanning approximately 7 km of forests on both sides of the road. Therefore, at least 20 km of forest roads could be scanned in one day. When using the estimates from two zones (e.g., from 20 to 30 m and 30–40 m), the survey yields two sections, 20 m × 20 km, totaling 80 ha of scanned forest per day. In comparison, using traditional forest inventory methods, the same crew would measure approximately 10 circular plots, with a radius of 10 m, per day, yielding approximately 0.31 ha of inventoried area.

The choice of zones to use as reference data depends mostly on the edge effect and accuracy loss due to the distance from the sensor. First, it is important to make sure that the trees used as reference to train models are not under edge influence. Harper et al. (2015) suggested that boreal forests are less affected by both natural and human-caused edges, with the edge effect influence rarely exceeding 20 m in parameters such as basal area and canopy cover. Second, the low accuracy of the predictions in the zones from 40 to 60 m indicates that these areas are less suitable as reference for, e.g., remote sensing-based models. With the proposed sensor configuration, the data acquired at 20–40 m from the road or stand's edge had the highest overall accuracy, being the most recommended for use as reference for model calibration.

The algorithm we describe is easy to implement. The parameters
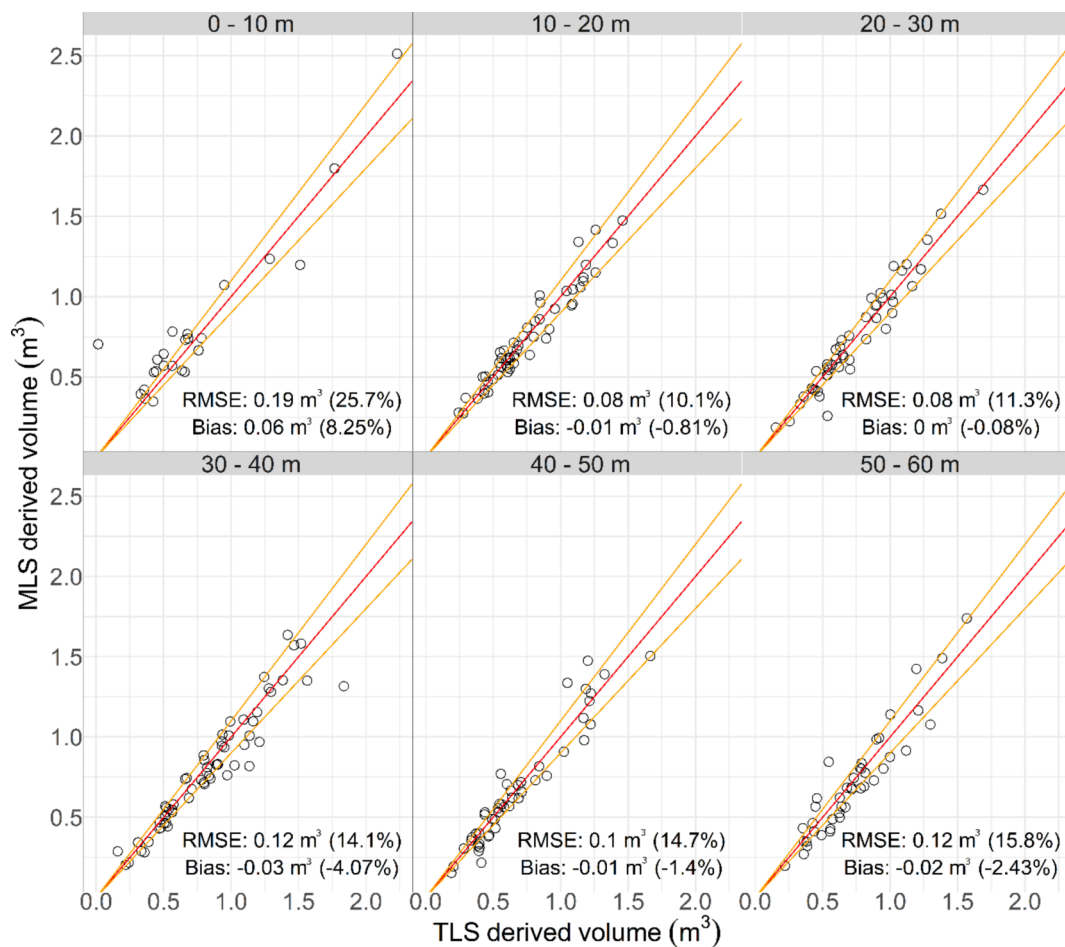
**Fig. 11.** Reference (TLS) vs. estimated (MLS) stem volume, in m$^3$. The red line is the 1:1 line, where reference and estimated values are equal. The orange lines represent a 10% deviation from the 1:1 line. RMSE = Root Mean Square Error. (For interpretation of the references to colour in this figure legend, the reader is referred to the web version of this article.)

**Table 3**

RMSE and bias of total volume estimates together with the average proportion of reference volume detected in each zone. The relative values were calculated using the reference total volume.

| Zone | RMSE | Bias | Average Proportion of Reference Volume Detected (±SD) |
|---|---|---|---|
| 0–10 m | 1.00 m$^3$ ∼ 27.2% | 0.48 m$^3$ ∼ 13.1% | 113% (±22.7%) |
| 10–20 m | 0.64 m$^3$ ∼ 8.33% | −0.42 m$^3$ ∼ -5.47% | 94.2% (±6.69%) |
| 20–30 m | 0.50 m$^3$ ∼ 7.97% | 0.07 m$^3$ ∼ 1.20% | 98.5% (±8.98%) |
| 30–40 m | 0.86 m$^3$ ∼ 8.96% | −0.50 m$^3$ ∼ -5.21% | 94.0% (±9.52%) |
| 40–50 m | 0.65 m$^3$ ∼ 10.5% | −0.54 m$^3$ ∼ -8.82% | 87.5% (±12.3%) |
| 50–60 m | 2.6 m$^3$ ∼ 39.5% | −2.24 m$^3$ ∼ -30.9% | 66.6 % (±14.8%) |

used, including angular step width and average distance between scan lines, were mostly derived from the survey's setup, enabling implementation in different forest conditions without the need of further parametrization. However, the difference in the accuracy of the analyzed variables in the different zones suggests that the algorithm's performance could be enhanced by using zone specific parameters.

## 5. Conclusions

In this study, we propose an algorithm to extract stem attributes from a car-mounted MLS circulating on forest roads, with focus on quantitative forest attributes such as DBH and stem volume in boreal forest conditions. Furthermore, we analyzed its performance at different distance ranges from the roadside. The results indicate that the proposed method can be an alternative for efficient reference data collection in forest inventories. With the presented sensor set up and algorithm, we were able to reduce the bias despite the proximity to the road by reaching beyond the forest area under edge effect. In addition, the accuracy of DBH and stem profile estimates remained stable from 10 to 60 m from the road, with the presence of few outliers. However, the accuracy of individual tree detection and stem volume estimates decreases as the distance from the road increases. Finally, future work might focus on improving branch filtering and explore how the predictions can be used to train remote sensing-based models in large-scale forest inventories.

*CRediT authorship contribution statement*

**Raul de Paula Pires:** Methodology, Software, Validation, Formal analysis, Writing – original draft, Visualization. **Kenneth Olofsson:** Methodology, Software, Validation, Resources, Writing – review & editing, Supervision. **Henrik Persson:** Methodology, Resources, Writing – review & editing, Supervision. **Eva Lindberg:** Methodology, Resources, Writing – review & editing, Supervision. **Johan Holmgren:**

Conceptualization, Methodology, Software, Resources, Writing – review & editing, Supervision, Funding acquisition.

**Declaration of Competing Interest**

The authors declare that they have no known competing financial interests or personal relationships that could have appeared to influence the work reported in this paper.

**References**

Axelsson, T., Bengtsson, P., Blomqvist, G., Landström, A., Melin, A., Fries, C., Möller, L., Holmström, A., 2018. Infrastruktur i skogsbruket med betydelse för skogsproduktionen : Nuläge och åtgärdsförslag. Delrapport inom Samverkan för ökad skogsproduktion. Skogsstyrelsen Rapp. 3, 42.

Bakula, M., Przestrzelski, P., Kazmierczak, R., 2015. Reliable technology of centimeter GPS/GLONASS surveying in forest environments. IEEE Trans. Geosci. Remote Sens. 53 (2), 1029–1038. https://doi.org/10.1109/TGRS.2014.2332372.

Balenović, I., Liang, X., Jurjević, L., Hyyppä, J., Seletković, A., Kukko, A., 2020. Hand-held personal laser scanning – current status and perspectives for forest inventory application. Croat. J. For. Eng. 42, 165–183. https://doi.org/10.5552/crojfe.2021.858.

Bienert, A., Georgi, L., Kunz, M., Maas, H.G., von Oheimb, G., 2018. Comparison and combination of mobile and terrestrial laser scanning for natural forest inventories. Forests 8, 1–25. https://doi.org/10.3390/f9070395.

Calders, K., Adams, J., Armston, J., Bartholomeus, H., Bauwens, S., Bentley, L.P., Chave, J., Danson, F.M., Demol, M., Disney, M., Gaulton, R., Krishna Moorthy, S.M., Levick, S.R., Saarinen, N., Schaaf, C., Stovall, A., Terryn, L., Wilkes, P., Verbeeck, H., 2020. Terrestrial laser scanning in forest ecology: Expanding the horizon. Remote Sens. Environ. 251, 112102. https://doi.org/10.1016/j.rse.2020.112102.

Čerňava, J., Mokroš, M., Tuček, J., Antal, M., Slatkovská, Z., 2019. Processing Chain for Estimation of Tree Diameter from GNSS-IMU-Based Mobile Laser Scanning Data. Remote Sens. 11, 615. https://doi.org/10.3390/rs11060615.

Delgado, J.D., Arroyo, N.L., Arévalo, J.R., Fernández-Palacios, J.M., 2007. Edge effects of roads on temperature, light, canopy cover, and canopy height in laurel and pine forests (Tenerife, Canary Islands). Landsc. Urban Plan. 81 (4), 328–340. https://doi.org/10.1016/j.landurbplan.2007.01.005.

Forsman, M., Börlin, N., Olofsson, K., Reese, H., Holmgren, J., 2018. Bias of cylinder diameter estimation from ground-based laser scanners with different beam widths: A simulation study. ISPRS J. Photogramm. Remote Sens. 135, 84–92. https://doi.org/10.1016/j.isprsjprs.2017.11.013.

Forsman, M., Holmgren, J., Olofsson, K., 2016. Tree stem diameter estimation from mobile laser scanning using line-wise intensity-based clustering. Forests 7, 206. https://doi.org/10.3390/f7090206.

Hamraz, H., Jacobs, N.B., Contreras, M.A., Clark, C.H., 2019. Deep learning for conifer/ deciduous classification of airborne LiDAR 3D point clouds representing individual trees. ISPRS J. Photogramm. Remote Sens. 158, 219–230. https://doi.org/10.1016/j.isprsjprs.2019.10.011.

Harper, K.A., Macdonald, S.E., Mayerhofer, M.S., Biswas, S.R., Esseen, P.A., Hylander, K., Stewart, K.J., Mallik, A.U., Drapeau, P., Jonsson, B.G., Lesieur, D., Kouki, J., Bergeron, Y., 2015. Edge influence on vegetation at natural and anthropogenic edges of boreal forests in Canada and Fennoscandia. J. Ecol. 103, 550–562. https://doi.org/10.1111/1365-2745.12398.

Holmgren, J., Tulldahl, M., Nordlöf, J., Willén, E., Olsson, H., 2019. Mobile laser scanning for estimating tree stem diameter using segmentation and tree spine calibration. Remote Sens. 11, 1–18. https://doi.org/10.3390/rs11232781.

Holopainen, M., Vastaranta, M., Hyyppä, J., 2014. Outlook for the next generation's precision forestry in Finland. Forests 5, 1682–1694. https://doi.org/10.3390/f5071682.

Hopkinson, C., Chasmer, L., Young-Pow, C., Treitz, P., 2004. Assessing forest metrics with a ground-based scanning lidar. Can. J. For. Res. 34 (3), 573–583. https://doi.org/10.1139/x03-225.

Hunčaga, M., Chudá, J., Tomaštík, J., Slámová, M., Koreň, M., Chudý, F., 2020. The comparison of stem curve accuracy determined from point clouds acquired by different terrestrial remote sensing methods. Remote Sens. 12 (17), 2739. https://doi.org/10.3390/rs12172739.

Hyyppä, E., Hyyppä, J., Hakala, T., Kukko, A., Wulder, M.A., White, J.C., Pyörälä, J., Yu, X., Wang, Y., Virtanen, J.P., Pohjavirta, O., Liang, X., Holopainen, M., Kaartinen, H., 2020a. Under-canopy UAV laser scanning for accurate forest field measurements. ISPRS J. Photogramm. Remote Sens. 164, 41–60. https://doi.org/10.1016/j.isprsjprs.2020.03.021.

Hyyppä, E., Kukko, A., Kaijaluoto, R., White, J.C., Wulder, M.A., Pyörälä, J., Liang, X., Yu, X., Wang, Y., Kaartinen, H., Virtanen, J.P., Hyyppä, J., 2020b. Accurate derivation of stem curve and volume using backpack mobile laser scanning. ISPRS J. Photogramm. Remote Sens. 161, 246–262. https://doi.org/10.1016/j.isprsjprs.2020.01.018.

Hyyppä, E., Yu, X., Kaartinen, H., Hakala, T., Kukko, A., Vastaranta, M., Hyyppä, J., 2020c. Comparison of backpack, handheld, under-canopy UAV, and above-canopy UAV laser scanning for field reference data collection in boreal forests. Remote Sens. 12, 1–31. https://doi.org/10.3390/rs12203327.

Kolendo, Ł., Kozniewski, M., Ksepko, M., Chmur, S., Neroj, B., 2021. Parameterization of the individual tree detection method using large dataset from ground sample plots and airborne laser scanning for stands inventory in coniferous forest. Remote Sens. 13 (14), 2753. https://doi.org/10.3390/rs13142753.

Kukko, A., Kaijaluoto, R., Kaartinen, H., Lehtola, V.V., Jaakkola, A., Hyyppä, J., 2017. Graph SLAM correction for single scanner MLS forest data under boreal forest canopy. ISPRS J. Photogramm. Remote Sens. 132, 199–209. https://doi.org/10.1016/j.isprsjprs.2017.09.006.

Lau, A., Bentley, L.P., Martius, C., Shenkin, A., Bartholomeus, H., Raumonen, P., Malhi, Y., Jackson, T., Herold, M., 2018. Quantifying branch architecture of tropical trees using terrestrial LiDAR and 3D modelling. Trees - Struct. Funct. 32 (5), 1219–1231. https://doi.org/10.1007/s00468-018-1704-1.

Liang, X., Hyyppä, J., Kaartinen, H., Lehtomäki, M., Pyörälä, J., Pfeifer, N., Holopainen, M., Brolly, G., Francesco, P., Hackenberg, J., Huang, H., Jo, H.W., Katoh, M., Liu, L., Mokroš, M., Morel, J., Olofsson, K., Poveda-Lopez, J., Trochta, J., Wang, D., Wang, J., Xi, Z., Yang, B., Zheng, G., Kankare, V., Luoma, V., Yu, X., Chen, L., Vastaranta, M., Saarinen, N., Wang, Y., 2018a. International benchmarking of terrestrial laser scanning approaches for forest inventories. ISPRS J. Photogramm. Remote Sens. 144, 137–179. https://doi.org/10.1016/j.isprsjprs.2018.06.021.

Liang, X., Kukko, A., Hyyppä, J., Lehtomäki, M., Pyörälä, J., Yu, X., Kaartinen, H., Jaakkola, A., Wang, Y., 2018b. In-situ measurements from mobile platforms: An emerging approach to address the old challenges associated with forest inventories. ISPRS J. Photogramm. Remote Sens. 143, 97–107. https://doi.org/10.1016/j.isprsjprs.2018.04.019.

Lindberg, E., Holmgren, J., Olofsson, K., Olsson, H., 2012. Estimation of stem attributes using a combination of terrestrial and airborne laser scanning. Eur. J. For. Res. 131 (6), 1917–1931. https://doi.org/10.1007/s10342-012-0642-5.

Liu, L., Zhang, A., Xiao, S., Hu, S., He, N., Pang, H., Zhang, X., Yang, S., 2021. Single Tree Segmentation and Diameter at Breast Height Estimation with Mobile LiDAR. IEEE Access 9, 24314–24325. https://doi.org/10.1109/ACCESS.2021.3056877.

Lovell, J.L., Jupp, D.L.B., Culvenor, D.S., Coops, N.C., 2003. Using airborne and ground-based ranging lidar to measure canopy structure in Australian forests. Can. J. Remote Sens. 29 (5), 607–622. https://doi.org/10.5589/m03-026.

Maltamo, M., Hauglin, M., Næsset, E., Gobakken, T., 2019. Estimating stand level stem diameter distribution utilizing harvester data and airborne laser scanning. Silva Fenn. 53, 1–19. https://doi.org/https://doi.org/10.14214/sf.10075.

Næsset, E., 2002. Predicting forest stand characteristics with airborne scanning laser using a practical two-stage procedure and field data. Remote Sens. Environ. 80 (1), 88–99. https://doi.org/10.1016/S0034-4257(01)00290-5.

Newnham, G.J., Armston, J.D., Calders, K., Disney, M.I., Lovell, J.L., Schaaf, C.B., Strahler, A.H., Danson, F.M., 2015. Terrestrial laser scanning for plot-scale forest measurement. Curr. For. Rep. 1 (4), 239–251. https://doi.org/10.1007/s40725-015-0025-5.

Olofsson, K., Holmgren, J., 2016. Single tree stem profile detection using terrestrial laser scanner data, flatness saliency features and curvature properties. Forests 7, 207. https://doi.org/10.3390/f7090207.

Olofsson, K., Holmgren, J., Olsson, H., 2014. Tree stem and height measurements using terrestrial laser scanning and the RANSAC algorithm. Remote Sens. 6, 4323–4344. https://doi.org/10.3390/rs6054323.

Packalén, P., Maltamo, M., 2008. Estimation of species-specific diameter distributions using airborne laser scanning and aerial photographs. Can. J. For. Res. 38 (7), 1750–1760. https://doi.org/10.1139/X08-037.

Pierzchała, M., Giguère, P., Astrup, R., 2018. Mapping forests using an unmanned ground vehicle with 3D LiDAR and graph-SLAM. Comput. Electron. Agric. 145, 217–225. https://doi.org/10.1016/j.compag.2017.12.034.

Puente, I., González-Jorge, H., Martínez-Sánchez, J., Arias, P., 2013. Review of mobile mapping and surveying technologies. Meas. J. Int. Meas. Confed. 46 (7), 2127–2145. https://doi.org/10.1016/j.measurement.2013.03.006.

Puliti, S., Breidenbach, J., Astrup, R., 2020. Estimation of forest growing stock volume with UAV laser scanning data: Can it be done without field data? Remote Sens. 12, 1245. https://doi.org/10.3390/RS12081245.

Pyörälä, J., Kankare, V., Liang, X., Saarinen, N., Rikala, J., Kivinen, V.P., Sipi, M., Holopainen, M., Hyyppä, J., Vastaranta, M., 2019a. Assessing log geometry and wood quality in standing timber using terrestrial laser-scanning point clouds. Forestry 92, 177–187. https://doi.org/10.1093/forestry/cpy044.

Pyörälä, J., Saarinen, N., Kankare, V., Coops, N.C., Liang, X., Wang, Y., Holopainen, M., Hyyppä, J., Vastaranta, M., 2019b. Variability of wood properties using airborne and terrestrial laser scanning. Remote Sens. Environ. 235, 111474. https://doi.org/10.1016/j.rse.2019.111474.

Qian, C., Liu, H., Tang, J., Chen, Y., Kaartinen, H., Kukko, A., Zhu, L., Liang, X., Chen, L., Hyyppä, J., 2017. An integrated GNSS/INS/LiDAR-SLAM positioning method for

highly accurate forest stem mapping. Remote Sens. 9, 1–16. https://doi.org/10.3390/rs9010003.

Reynolds, M.R., Burk, T.E., Huang, W.-C., 1988. Goodness-of-fit tests and model selection procedures for diameter distribution models. For. Sci. 34 (2), 373–399. https://doi.org/10.1093/forestscience/34.2.373.

Roussel, J.-R., Auty, D., Coops, N.C., Tompalski, P., Goodbody, T.R.H., Meador, A.S., Bourdon, J.-F., de Boissieu, F., Achim, A., 2020. lidR: An R package for analysis of Airborne Laser Scanning (ALS) data. Remote Sens. Environ. 251, 112061. https://doi.org/10.1016/j.rse.2020.112061.

Skudnik, M., Jevšenak, J., 2022. Artificial neural networks as an alternative method to nonlinear mixed-effects models for tree height predictions. For. Ecol. Manage. 507, 120017. https://doi.org/10.1016/j.foreco.2022.120017.

Xi, Z., Hopkinson, C., Rood, S.B., Peddle, D.R., 2020. See the forest and the trees: Effective machine and deep learning algorithms for wood filtering and tree species classification from terrestrial laser scanning. ISPRS J. Photogramm. Remote Sens. 168, 1–16. https://doi.org/10.1016/j.isprsjprs.2020.08.001.

Zhang, C., Jiang, Y., Xu, B., Li, X., Zhu, Y., Lei, L., Chen, R., Dong, Z., Yang, H., Yang, G., 2020. Apple tree branch information extraction from terrestrial laser scanning and backpack-LiDAR. Remote Sens. 12, 1–17. https://doi.org/10.3390/rs12213592.

Zhang, W., Qi, J., Wan, P., Wang, H., Xie, D., Wang, X., Yan, G., 2016. An easy-to-use airborne LiDAR data filtering method based on cloth simulation. Remote Sens. 8, 1–22. https://doi.org/10.3390/rs8060501.

Zhen, Z., Quackenbush, L.J., Zhang, L., 2016. Trends in automatic individual tree crown detection and delineation-evolution of LiDAR data. Remote Sens. 8, 1–26. https://doi.org/10.3390/rs8040333.